Journal of Colloid and Interface Science 658 (2024) 52–60

Contents lists available at ScienceDirect

Journal of Colloid And Interface Science

journal homepage: www.elsevier.com/locate/jcis

Regular Article

Electro-optics of confined systems

Ana Cazorla, Sergio Martín-Martín, Ángel V. Delgado, María L. Jiménez *

Department of Applied Physics, University of Granada, Avda. de Fuente Nueva sn, 18071, Granada, Spain

GRAPHICAL ABSTRACT

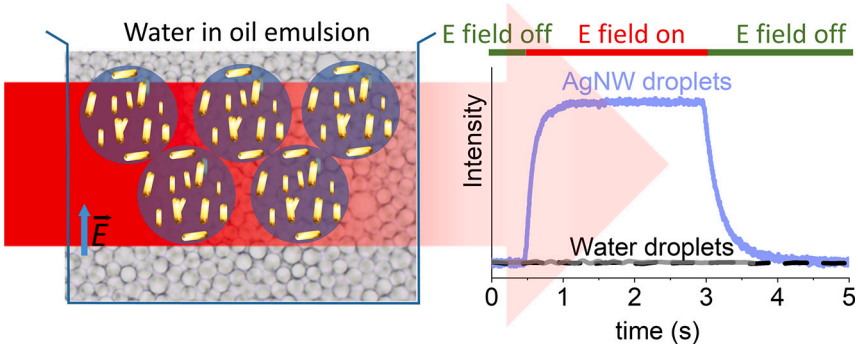

ARTICLE INFO

Keywords:
Confinement effects
Electric birefringence
Electro-orientation
Silver nanowires
Sodium montmorillonite

ABSTRACT

Confinement in microenvironments occurs in many natural systems and technological applications. However, little is known about the behaviour of the immersed nanoparticles. In this work we show that their diffusion, electro-orientation and electric field induced polarization can be determined through electric birefringence experiments. We analyze aqueous dispersions of silver nanowires and clay particles confined inside microdroplets. We have observed that confinement reduces the amount of particles that can be oriented by the external electric field. However, the polarizability of the oriented particles is not affected by the presence of the oil/water boundary, and it is the same as in unbounded media, which agrees with the fact that the electric polarization and related phenomena are short-ranged.

1. Introduction

Although a general definition is not easy, and it is rather system dependent, we can say that a medium is confined when the dimensions of the sample itself are comparable to a natural length scale of the system. In such cases, the dynamics of the included particles may be determined by the presence of boundaries, this affecting many technological processes such as extrusion, bearing lubrication, or inkjet printing [1,2]. Confinement refers not only to geometry, but in general to limitations in the volume of phase space accessible to the particles, as when they are forced to follow the channels of a porous material [3]. In fact, due to Brownian diffusion, convection and chemical interactions, nanoparticles enclosed in microdroplets may explore the surrounding media in a different manner than in unbounded medium, this affecting the behaviour of the particles despite the small ratio between their size and that of the droplets.

* Corresponding author.
E-mail addresses: acazorla@correo.ugr.es (A. Cazorla), sergiomartin96@correo.ugr.es (S. Martín-Martín), adelgado@ugr.es (Á.V. Delgado), jimenezo@ugr.es (M.L. Jiménez).

https://doi.org/10.1016/j.jcis.2023.11.180
Received 22 June 2023; Received in revised form 13 November 2023; Accepted 28 November 2023
Available online 5 December 2023

Confinement in spherical compartments also occurs in many natural environments. Suffice it to mention that 40% of the cell volume, where living processes take place, is occupied by macromolecules [4,5]. On the other hand, increased attention to microreactors and droplet microfluidics [6] has led to the discover of unique phenomena that do not take place in unbounded media, such as the acceleration of enzymatic and organic reactions [7], spontaneous molecule reduction [8] and ion transfer [9], to mention a few. Chamberlayne et al. [10] have shown that chemical reactions are enhanced in small microdroplets because of the electric field associated to the water/oil interface. In fact, these authors found that the electric field close to the interface is enhanced for small microdroplets, this probably due to the excess of unpaired ions (that is, those ions generated in the surfactant polar head dissociation).

Microdroplets can be used as platforms for nanoparticle synthesis [11,12], sensors [13], micromotors [14] or drug transport and delivery systems [15]. However, apart from some interesting work about particle reorganization inside the droplets [16–19], little is known of the behaviour of particles inside microdroplets, specially in the case where electric fields are applied. This may be important because electric fields are used in several applications, since they promote transport, sorting and reorganization of droplets [20–22], active mixing [23], or destabilization of the surfactant layer and droplet fusion [24].

The interest in these systems comes from the broad-range of applications that have been found for nanoparticles in unbounded media. For instance, once the particles are driven out of their equilibrium structure by application of external fields, particle interactions between each other or with the sample limits produce new structures [25,26], and they can modulate the optical [27,28] and rheological [29] properties of the system, due to the electric field-induced dipole of the particles.

If particles are confined inside microdroplets, we cannot expect to probe their behaviour using the standard electrokinetic methods, such as electrophoresis, that will collect the response of the microdroplet itself, instead of that of the confined particles. Furthermore, the produced emulsions are far from equilibrium, since buoyancy usually produces a phase separation between a concentrated emulsion, where the microdroplets are tightly packed, and the solution. One alternative is the visual inspection with a microscope, but this method precludes the study of nanoparticles or the majority of macromolecules such as polymers.

A possible approach is the electric birefringence technique applied to electro-oriented anisotropic particles. Due to thermal randomization, the system is only partially oriented. The degree of alignment can be quantified by the orientational order parameter S, defined as

$$S = \frac{1}{2}\langle 3\cos^2\theta - 1\rangle = \frac{1}{2}\int_0^{\pi} 2\pi\left(3\cos^2\theta - 1\right)\sin\theta f(\theta)\mathrm{d}\theta \tag{1}$$

where θ is the angle between the field that produces the orientation and the symmetry axis of the particle, the angle brackets indicate the average over the ensemble and $f(\theta)$ is the orientation distribution. Interestingly, when particles are aligned, the system becomes birefringent, that is, the refractive index in the direction parallel to the field ($n_{\parallel}$) differs from that in the perpendicular direction ($n_{\perp}$). The birefringence, i.e., the optical anisotropy $\Delta n = n_{\parallel} - n_{\perp}$ is related to the orientational order parameter as [30]:

$$\Delta n = \Delta n_{\mathrm{sat}} S \tag{2}$$

where Δn_{sat} is the value of Δn attained when the symmetry axes of all the particles are perfectly aligned with the direction of the external field. This technique has been widely used to analyze the spectral response of macromolecules immersed in an unbounded solution [28,31–37]. Much is already known about the behaviour of both rigid particles and flexible polymers under the effect of an electric field of varying intensity and frequency. Less is known about the response of these systems when the particles are in a confined medium. In this work, a method is presented to obtain the electrokinetic response of individual nanoparticles within microdroplets. It is intended to analyze whether confinement affects the behaviour of this emulsion, in which the ratio between particle and droplet size is small, and how the electrokinetic response depends on the characteristics of the particles and the medium. The proposed method is the determination of the electrical birefringence of silver nanowires and sodium montmorillonite confined in aqueous microdroplets under the action of alternating electric fields of varying frequency and intensity. Both microfluidics and vigorous stirring methods will be used to encapsulate the particles in the droplets.

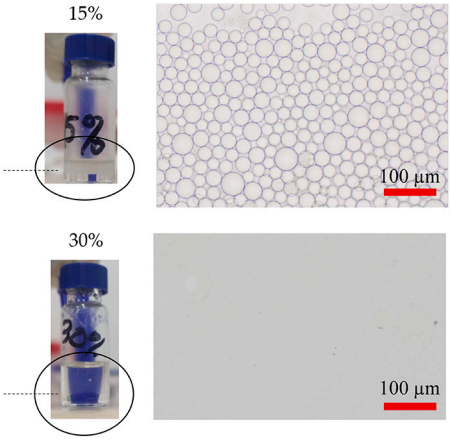

Fig. 1. Left column: Images of the containers with the emulsion in two cases: 15% (top) and 30% of RIM (bottom). The dashed lines indicate the position of the interface between emulsion and oil. Right column: Microscope photos of the emulsion.

2. Materials and methods

2.1. Materials

The system is a water in oil (W/O) emulsion. The outer phase is a mixture of an hydrofluoroether, HFE-7500 (HFE hereafter, HFE-7500 3M (TM) Novec (TM) Engineered fluid, Fluorochem, UK), and a 0.4% v/v surfactant (TAX hereafter, FluoroSurf^{TM}, Emulseo, Darwin, France). This fluorinated oil is usually employed as the continuous phase, since its viscosity is low, it is transparent and its refractive index and density are very similar to those of water, and hence, the turbidity of the emulsion is small whatever the size of the droplets.

Despite the refractive index of HFE, $n_{\mathrm{O}} = 1.290$, is similar to that of water ($n_{\mathrm{W}} = 1.333$), the small difference is enough to have a significant light scattering from the water/oil interface. In order to decrease the turbidity of the samples we added 1-3bis(trifluoromethyl)-5-bromobenzene (RIM hereafter, Merck, Germany, purity 99%, $n_{\mathrm{RIM}} = 1.427$). In Fig. 1 we show an example. The interface of the droplets is clearly visible when the concentration of RIM is lower than 30%, but it becomes nearly invisible when the concentration of RIM is raised up to 30%.

The inner phase of the emulsion was an aqueous suspension of commercial silver nanowires (Agnws, Plasma Chem Laboratory, Germany), or of sodium montmorillonite (NaMt). The latter was obtained by sodium homoionization of bentonite (purchased from Sigma-Aldrich, USA). The resulting particles are lamellar with negative charge on their faces and pH-dependent charge on their edges. They were characterized by environmental scanning electron microscopy. Their average diameter is $D_{NaMt} = (1.7 \pm 0.6)$ μm [38].

Regarding the Agnws elongated particles, in Fig. S1 we show transmission electron microscope pictures with two magnifications. From measurements in different pictures, the histograms included in the Figure were obtained. The size distributions of both axes fit well to log-normal distributions. It is concluded that the diameter and length are,

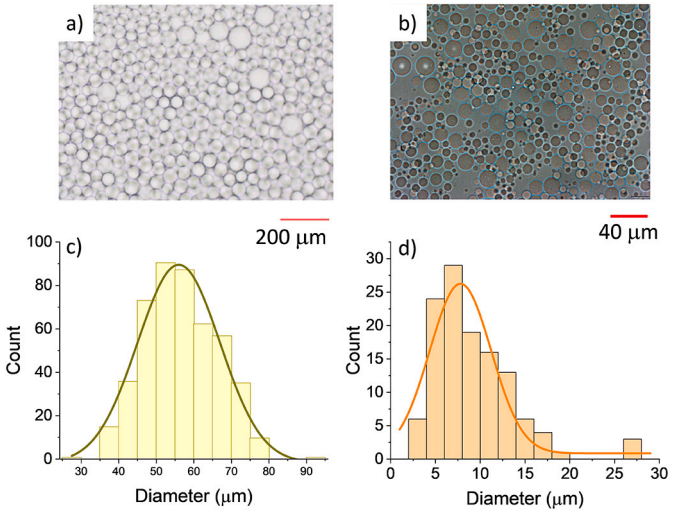

Fig. 2. a) and c) Agnw/HFE emulsion produced with microfluidics techniques and size histogram, respectively. b) and d) Picture and histogram of the NaMt droplets obtained by the stirring method.

respectively, $D_{Agnw} = (44 \pm 18)$ nm and $L_{AgNw} = (2.0 \pm 0.9)$ µm, where the standard deviation has been used again as uncertainty.

Agnws as received are dispersed in isopropanol. So, in order to change the dispersing medium to a water solution, the protocol described in SI was followed.

2.2. Experimental methods

2.2.1. Microdroplet generator

Emulsification is achieved with a commercial droplet generator chip (Elveflow, France) based on the flow focusing technique. With this technique, the outer and inner medium of the emulsion are flown through the microfluidic chip microchannels and converge in one point. By adjusting the flow rate of both liquids, droplets of homogeneous size can be obtained. Droplet generation based on microfluidic methods has the advantage of a high monodispersity. An example is shown in Fig. 1, with an average droplet diameter of 56 µm and a standard deviation of 9 µm. With this procedure, we confirmed that emulsions remained stable for over 2 weeks (in fact, the photographs in Fig. 1 were taken one week after preparation). In all cases, the emulsions were investigated the next day after preparation. Figs. 2a,c show, respectively, a picture of the Agnws microdroplets immersed in HFE (Agnws/HFE hereafter) and a size histogram.

Emulsions of NaMt particles were also prepared by vigorous stirring of a mixture of both 1 mL of the mixture of oil and surfactant with 1 mL of the NaMt solution with an IKA T10 basic ULTRA-TURRAX homogenizer (20 seconds at 15000 rpm). In Fig. 2b, d we present a microscope photo and the size histogram of the obtained emulsion. In this case, the size dispersion is larger, but smaller droplets (diameter 9 ± 5 µm, the error being estimated by the standard deviation) can be produced. Hereafter, 56 µm (made with microfluidic techniques) and 9 µm (made by vigorous stirring) emulsions will be called NaMt/HFE56 and NaMt/HFE9, respectively.

2.2.2. Electric birefringence device

The birefringence measurements were performed with a homemade electro-optical setup consisting of a low-power He-Ne laser beam (Laser Products 05-LHP-151, USA), a polariser at 45°, the sample to be measured in a quartz Kerr cell (Starna Scientific, UK), a quarter-wave plate, an analyser at $-(45° + \alpha)$ and, finally, a photodiode connected to an oscilloscope. Sinusoidal electric pulses are applied to the suspension through vertical stainless steel electrodes. A commercial generator (Tektronix AFG 3101, USA) and an low frequency amplifier (Piezo Systems Inc. EPA-104, USA) are used. All the optical plates and the photodiode were purchased from Edmund Optics, UK. The setup has a water circuit to thermostat all the suspensions at 15 °C. This birefringence equipment is described in more detail elsewhere [38–40]. The transient birefringence is obtained from the change in light intensity collected by the photodiode upon application of the field, as follows:

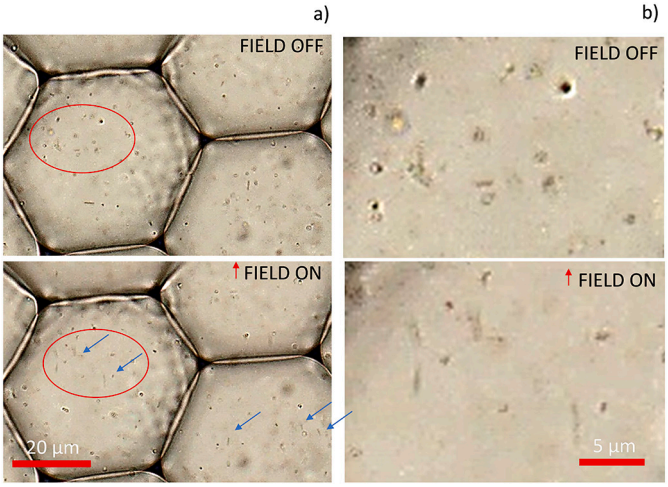

Fig. 3. a) Real-time observation of the electro-orientation of silver nanowires inside droplets immersed in HFE under a high frequency sinusoidal electric field. b) Detail of the selected area.

$$\Delta n(t) = \frac{\lambda}{\pi l}\left[\arcsin\left(\sqrt{\frac{A(t)}{A_o}}\sin\alpha\right) - \alpha\right] \quad (3)$$

being λ the wavelength of the laser beam, l the optical path length, A_0 the baseline oscilloscope signal when no field is applied and $A(t)$ the signal at time t. Every data point presented is the average of three repetitions.

The electro-orientation of the particles was also visually characterized with an optical microscope (CKX53 with a digital camera SC50, Olympus, Germany) equipped with a home-made cell with two aluminium paper electrodes of $d \sim 420$ µm spacing.

3. Results and discussion

3.1. Optical visualization of electric field-induced particle orientation

When spheroidal particles are subjected to an external electric field, it induces an electric dipole around them, this promoting the orientation of their longest axis along the field direction. Two contributions to electro-orientation are expected. On the one hand, the external electric field induces an electric dipole and produces a torque that drives the sample to some degree of orientation. In addition to the electric contribution, the existence of a hydrodynamic torque must be taken into account in some cases: the countercharge (that is, the excess of ions in the particle neighbourhood) migrates under the effect of the external electric field, dragging liquid through electro-osmotic fluxes. In the case of barely charged metallic particles, the ion accumulation at low frequencies induces some asymmetrical electro-osmotic fluxes [41–46], but this effect (so-called induced charge electro-osmosis, ICEO) has been shown to be negligible in the case of large salt content [28] and vanishes for AC fields in the MHz range [39,46].

Fig. 3 shows two frames of an Agnws/HFE emulsion placed on a coverslip between two parallel electrodes. The non-spherical shape of the droplets indicates a partial evaporation of the surrounding HFE. The top photo shows the system in equilibrium: we can observe several particles randomly oriented inside the droplets. In the bottom frame, an electric field is applied. The field provokes the nanowires electro-orientation and a large amount of particles align towards its direction.

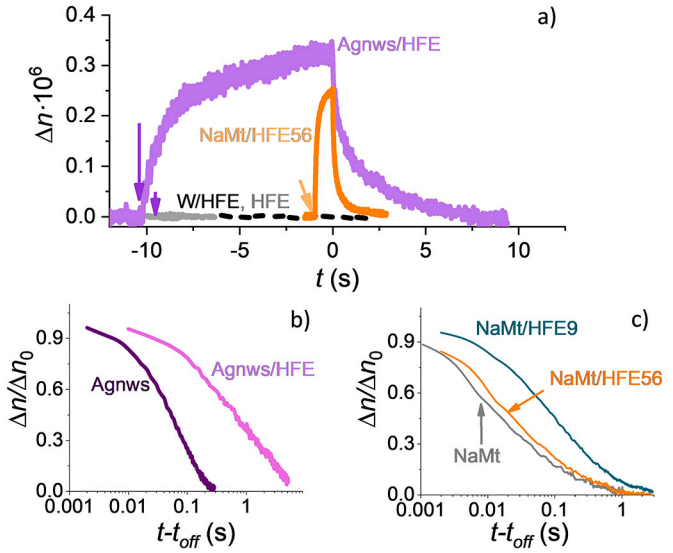

Fig. 4. a) Electric birefringence response of the emulsions indicated under a 1 MHz sinusoidal electric pulse of amplitude 20 V/mm (NaMt/HFE56), 15 V/mm (Agnws/HFE) and 40 V/mm (HFE and W/HFE emulsion). HFE (grey line) and W/HFE (black line) indicate the birefringence signal of the oil that remains below the droplets during the experiments and the response of a water in HFE oil emulsion without particles, respectively. The arrows indicate the electric field switching on. The field was switched off at $t = 0$. The experimental errors is 5×10^{-9}. b) Electric birefringence decay after switching off the electric field for Agnws in unbounded media and confined inside 56 μm droplets. The experimental error is less than 5%. c) The same but for NaMt in unbounded media and confined in 56 μm (NaMt/HFE56) and 9 μm (NaMt/HFE9) droplets.

Apparently, particle alignment is not hindered by the confinement and the system randomizes when the electric field is removed.

3.2. Electric birefringence dynamics

In Fig. 4a we show the dynamics of the electric birefringence of the NaMt/HFE56 and Agnws/HFE emulsions. The response is similar to previous results reported in [28,33,38,39,47]. After switching on the electric field, particles orient and the electric birefringence of the sample increases until it reaches a stationary value Δn_0. Once the field is removed, the sample takes a time to randomize and the transient birefringence goes to zero in an stretched-exponential-type decay:

$$\Delta n(t) = \Delta n_0 \exp\left[-(t/\tau)^s\right] \tag{4}$$

being s the stretched exponent accounting for the polydispersity of the sample and τ the relaxation time, related to the rotational diffusion coefficient Θ through

$$\langle\tau\rangle = 1/6\Theta \tag{5}$$

where $\langle\tau\rangle = \frac{\Gamma[1/s]}{s}\tau$, Γ is the Euler gamma function and Θ depends on the particle geometry and the rheological properties of the medium:

$$\Theta = \frac{3k_BT}{\pi\eta_m R^3} F_\Theta \tag{6}$$

Here η_m is the viscosity of the host fluid, R is the length of the long axis of the particles, k_BT is the thermal energy and F_Θ is a geometrical factor that depends on their shape [48].

By visual inspection we did not detect any nanowire dispersed in the continuous oil phase (see Fig. S2 for an example, where only a few dots are observed in the oil). Electric birefringence experiments in the bottom part of the cell, where there are no droplets showed a minor response (Fig. 4a, grey line labelled "HFE"), this confirming that the majority of the particles remain inside the droplets. We also observe a negligible response in the case of W/HFE emulsion, that is, droplets without particles inside (Fig. 4a, black line labelled W/HFE), confirming that the birefringence signal comes from the particles and not from the droplets themselves. This was expected, since the latter have spherical shape, and hence no orientation is expected for them. Note that our results confirm that the electric field is too low to produce a significant deformation of the shape of the droplets, this probably due to the large W/O interfacial tension, as observed previously for electric fields below roughly 100 V/mm [49,50].

In Fig. 4b and c we compare the birefringence decay after switching off the electric field when particles are in an unbounded medium and confined in the microdroplets. From the unbounded media cases, and fitting the experimental results to Eq. (4) we obtain a characteristic time decay of $\langle\tau\rangle = (0.070 \pm 0.02)$ s and (0.0925 ± 0.004) s for Agnws and NaMt, respectively. By using Eq. (6) we obtain that the average length of the suspended Agnws is $L_{Agnw} = (1.68 \pm 0.01)$ μm, and the average diameter $D_{NaMt} = (1.15 \pm 0.03)$ μm for NaMt, close to the TEM determinations.

In the case of confined Agnws (Fig. 4b) the response is slower. From visual inspection (see Fig. 3 and Fig. S2 in Supplementary Information for further examples) we did not detect particle aggregation. On the other hand, this slowing down could be attributed to a selectivity in the droplets formation procedure. Such effect is not observed in the case of NaMt/HFE56 (which correspond to microfluidic-produced 56 μm droplets of NaMt in HFE) but it occurs in the case of NaMt/HFE9, which correspond to the 9 μm NaMt droplets made by vigorous stirring of the mixture HFE and NaMt (Fig. 4c). With the latter procedure we can be sure that the particle size distribution inside the droplets is the same as in the unbounded systems, this confirming that the slowing-down effect is due to the confinement. Furthermore, the dispersion of the droplet size in the experiments is expected to be smaller than the value reported in the previous section, since the small contrast between water and HFE oil densities is enough to produce the buoyancy and packing of the droplets on the top of the cell, and we expect to have the small droplets above the larger ones. The fact that the slower response appears at smaller droplet size in the case of NaMt is in line with these particles being smaller than Agnws.

3.3. Particles oriented inside the microdroplets

When the applied field is strong enough, the particles have their major axis completely aligned with it and the birefringence of the system reaches its maximum value Δn_{MAX}. In the case of elongated particles, the major axis is the symmetry axis, and hence, this situation corresponds to $S = 1$. From the Clausius-Mossotti relation it can be deduced that [40]

$$\Delta n_{MAX} = \Delta n_{\text{sat}} = \frac{\phi\Delta\alpha^o}{2V_p n_m \varepsilon_0} \tag{7}$$

being ϕ the volume fraction of particles, n_m the refractive index of the solvent, V_p the particle volume, ε_0 the vacuum permittivity, and $\Delta\alpha^o$ is the optical polarizability anisotropy of the particles, defined as $\Delta\alpha^o = \alpha_l^o - \alpha_t^o$ (being l, t the directions parallel, perpendicular to the symmetry axis of the particle). If particles have an oblate shape, the major axis is perpendicular to the symmetry axis, and hence, upon application of strong fields, particles orient with the latter axis perpendicular to the field ($S = -0.5$), and by using Eq. (2) we have:

$$\Delta n_{MAX} = -0.5\Delta n_{\text{sat}} = -0.5\frac{\phi\Delta\alpha^o}{2V_p n_m \varepsilon_0} \tag{8}$$

On the other hand, for low and moderate electric fields, there is a partial orientation that depends on both the intensity of the electric field and the particle polarizability. In both Agnws and NaMt cases, since particles have an anisotropic shape, their polarization is not parallel to the external field, and as a consequence the field induces an electric torque that tends to align the particles along the external field. The stationary orientation distribution can be calculated as:

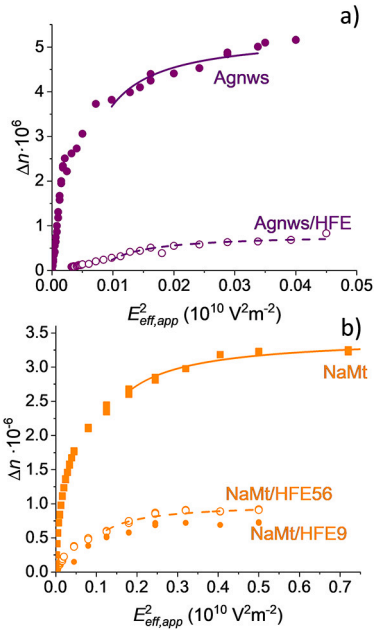

Fig. 5. Representation of electric birefringence saturation regime via application of sinusoidal electric fields of increasing amplitude of Agnws and Agnws/HFE (a), and NaMt, NaMt/HFE56 and NaMt/HFE9 (b). The experimental errors decrease from 6% at low field intensities to 0.5% at large intensities. Field frequency 1 MHz.

$$f(\theta) = \frac{\exp\left(U(\theta)/k_B T\right)}{\int_0^{\pi} 2\pi \exp\left(U(\theta)/k_B T\right) \sin(\theta)\, d\theta} \tag{9}$$

where the induced dipole interaction energy U depends on the orientation of the particles [51]:

$$U(\theta) = -\frac{1}{2}\Delta\alpha^e E^2_{eff,loc} \cos^2\theta \tag{10}$$

In Eq. (10), $\Delta\alpha^e = \alpha^e_l - \alpha^e_t$ is the electric polarizability anisotropy of the particles ($\alpha^e_{l(t)}$ is the polarizability of the particle along (perpendicular) to their symmetry axis) and $E_{eff,loc}$ the root mean square of the local electric field. In the case of moderate to large field strengths, it can be obtained an analytical expression for the integral in Eq. (1) and hence for the electric birefringence in Eq. (2). For instance [51–53],

$$\Delta n = \Delta n_{\mathrm{MAX}} \left(1 - \frac{3}{\gamma E^2_{eff,loc} - 1}\right) \tag{11}$$

being $\gamma = 1/E_c^2$, E_c the characteristic field at which saturation starts to take place ($E_c = \sqrt{\frac{2k_BT}{|\Delta\alpha^e|}}$). As we will see in the next section, the local electric field may differ from the applied one $E_{eff,app}$ by a certain factor $\beta = E_{eff,loc}/E_{eff,app}$ and hence:

$$\Delta n = \Delta n_{\mathrm{MAX}} \left(1 - \frac{3}{\gamma \beta^2 E^2_{eff,app} - 1}\right) \tag{12}$$

In Fig. 5 we show the electric birefringence of NaMt and Agnws, both immersed in an unbounded media and confined inside microdroplets, as a function of the square of the intensity of the applied field. We observe that the birefringence increases until it reaches its maximum value Δn_{MAX}. This saturation value is smaller when the particles are confined inside microdroplets. The saturation value of the birefringence is independent of the applied field (provided it is high enough) and only depends on the concentration of the particles ϕ and their optical and geometrical properties (see Eq. (7) for elongated particles and Eq. (8) for oblate ones). Since the particles are the same, the decrease in the saturation value can be explained by a decrease in the number of particles that can be aligned by the field.

Table 1
Experimental parameters of the fitting of Eq. (12) to the experimental results in Fig. 5.

System	$\Delta n_{\mathrm{MAX}} \cdot 10^6$	$\gamma\beta^2$ (10^{-9} m^2 V^{-2})	$\frac{\phi_{\mu d}}{\phi_{bulk}}$	β
NaMt Bulk	3.329 ± 0.017	2.64 ± 0.11		
NaMt/HFE	1.00 ± 0.02	0.80 ± 0.08	58%	0.55
Agnws Bulk	5.3 ± 0.1	109 ± 9		
Agnws/HFE	0.81 ± 0.04	54 ± 4	15%	0.6

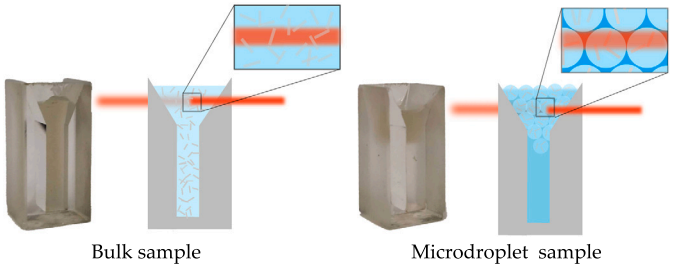

Fig. 6. Scheme of laser light propagation through unconfined and confined media.

The reduction in the number of oriented particles can be experimentally quantified from the data in Fig. 5. Fitting Eq. (12) to those data, we can determine Δn_{MAX} for both a controlled sample (for example a dispersion of particles with a controlled concentration, subscript *bulk* hereafter) and the emulsion (subscript μd) (see Table 1). Considering that (see Eqs. (7) and (8)):

$$\frac{\Delta n_{\mathrm{MAX},\mu d}}{\Delta n_{\mathrm{MAX},bulk}} = \frac{\phi_{\mu d}}{\phi_{bulk}} \tag{13}$$

We obtain the results in Table 1. As compared to an unbounded particle dispersion, the concentration of particles that are effectively oriented may decrease for three reasons. One is that microdroplets, and hence, the particles, do not fill all the space (see Fig. 6). However, due to the buoyancy of the droplets, they accumulate at the top of the Kerr cell, and hence, the fraction of volume struck by the laser beam should be about 64%. This reduction is similar to the concentration reduction $\phi_{\mu d}/\phi_{bulk}$ obtained in Table 1 for NaMt, but insufficient to explain the large birefringence reduction for Agnws.

A second reason is a possible decrease of the particle concentration during the droplets formation. In Fig. 5b we can see that using such two different emulsification methods we get similar results, this meaning that *i)* the concentration of particles does not vary due to emulsification, *ii)* the electro-orientation mechanisms are not affected by the droplet size.

Finally, the birefringence hindering for confined particles may be associated to a pinning effect of particles close to the W/O interface. The particles will arrange following the local shape, affecting their electric field-induced orientation in the neighbourhood of the droplet/HFE interface. In fact, in [18] it is shown that particles in electrospray-produced microdroplets tend to accumulate at the boundaries, this explaining the large amount of affected particles.

3.4. Electric field inside the microdroplets

In the previous section we have shown that Δn becomes independent of the electric field for large enough field intensities. On the other hand, at intermediate (Eq. (12)) and low field intensities (Kerr regime), the electric birefringence strongly depends on it. Hence, to characterize the electro-orientation of particles inside droplets it is mandatory to determine the local electric field.

In W/O emulsions, there are ions in the water phase, and hence there is a conductivity mismatch between the droplet and its surrounding oil medium. Under the application of an electric field $E_{eff,app}$, a non-

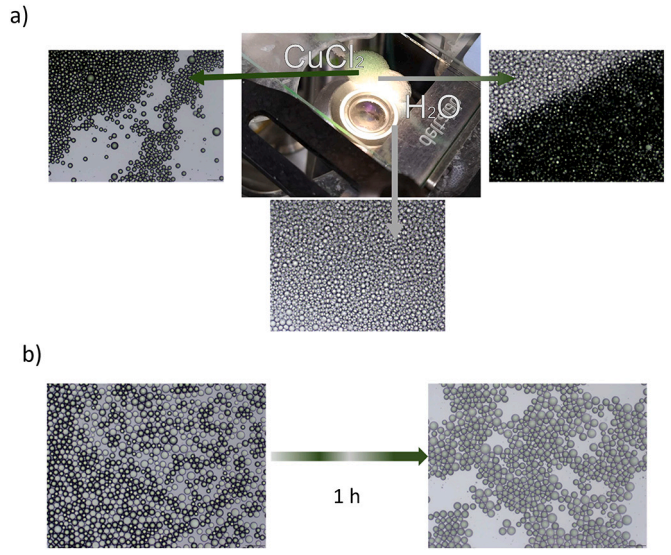

Fig. 7. a) Comparison of the contrast between droplets of $CuCl_2$ in HFE and pure water droplets in HFE. b) Mixture of $CuCl_2$ in HFE and pure water droplets right after preparation (left) and after 1 h (right). (For interpretation of the colours in the figure(s), the reader is referred to the web version of this article.)

equilibrium imbalance between the ionic fluxes inside and outside the drop is established, and ions of different sign accumulate at the opposite poles of the drop. This charge redistribution modifies the local electric field inside the drop. For alternating electric fields of frequency above the MHz range, ions have not enough time to redistribute upon every reversal of the electric field, and hence, this polarization phenomenon (so-called Maxwell-Wagner effect, [54]) is negligible, but at the MHz range and below the stationary state is reached and the local electric field $E_{eff,loc}$ is reduced to:

$$E_{eff,loc} = \frac{3K_O}{K_W + 2K_O} E_{eff,app} \tag{14}$$

where $K_O(K_W)$ is the conductivity of the oil (water) phase. In our case, the conductivity of the outer oil phase is negligible, and hence, the local electric field should vanish.

However, when droplets are packed, while particles are not observed to cross between two neighbour droplets, ions can do it and hence the electric field is not completely screened. The fact that particles are effectively oriented inside the droplets at these frequencies confirms that this is the case. In fact, it has been shown that it is possible to insert some molecules in already formed droplets [55–57]. Etienne et al. [58] have demonstrated that hydrophilic reagents, and even DNA strands of about 11 kbp are able to cross from one drop to the neighbour one through the oil phase, provided the distance between two neighbour droplets is short enough to promote the spontaneous formation of aqueous drops with diameters of the order of 100 nm in the oil phase.

In our case, the ionic transfer was further confirmed by mixing a water-in-HFE emulsion (W/HFE) with another one in which the droplets are made of a green $CuCl_2$ solution (Cu/HFE hereafter), clearly distinguishable from water droplets (see Fig. 7a). In these pictures we can see a clear difference between the droplets with and without $CuCl_2$. Fig. 7b shows the mixed emulsions, the droplets of $CuCl_2$ solution being clearly darker than water droplets. After 1 h, we observe no contrast between different droplets, indicating that diffusion of Cu^{2+} ions between neighbouring droplets has taken place, probably with the same mechanism as in Ref. [58], i.e., by the transient nucleation of tiny droplets that act as bridges for the ions between adjacent microdroplets.

In order to characterize the local electric field inside the droplets we can use the experimental data in Fig. 5. These data can be normalized to Δn_{MAX}, removing in this way the confinement effects on the number of oriented particles described in the previous section. On the other hand, the reduction in the local electric field is accounted by the factor β ($E_{eff,loc} = \beta E_{eff,app}$). Note also that γ and E_c in Eq. (12) only depend on the polarizability of the individual particles and hence, they are not affected by the confinement. Since $\beta = 1$ in the case of unbounded media, γ can be obtained by fitting Eq. (12) to the data of unbounded systems in Fig. 5. With these values, β (so $E_{eff,loc}$) can be obtained by fitting the experimental data of confined systems in Fig. 5 to Eq. (12) (see Table 1).

The obtained value for β (Table 1) is similar for both kinds of particles, which is not surprising considering that the ionic content of the droplets, responsible for the decrease in the local electric field, is also similar. Note that the electric field correction affects the x-axis and hence, it is independent of the asymptotic value of the birefringence Δn_{MAX}.

3.5. Electric birefringence spectra of Agnws

If the electric field is moderate and the electric energy is smaller than the thermal one, S and hence Δn are proportional to $E^2_{eff,loc}$: this is the so-called Kerr regime. Also, if the viscous torque can be neglected, then:

$$S/E^2_{eff,loc} = \frac{\Delta\alpha^e(\nu)}{30k_BT} \tag{15}$$

where ν is the field frequency.

The Kerr constant K is defined in this weak electric field regime as $K = \frac{\Delta n}{\lambda E^2_{eff,loc}}$. This quantity is plotted in Fig. 8a, where it has been normalized by the particle concentration c in g/L. The results are similar to those already reported [39]. At high frequency we observe a large birefringence, due to the metallic nature of the particles, highly polarizable. At low frequencies, the particle dipole induced by the external field is screened by the induced electric double layer and its contribution to the system birefringence relaxes to nearly zero [29,39,46].

As expected, we observe that the characteristic frequency at which the frequency dispersion of K occurs increases with the ionic strength (the NaCl concentrations are 0.3 mM and 0.1 mM for the systems with 200 mg/L and 400 mg/L particle concentration, respectively). As a consequence, the systems with 400 mg/L and smaller ionic strength *i)* exhibit a smaller relaxation frequency and *ii)* get oriented at low frequency due to a non negligible viscous torque produced by the asymmetric induced charge electroosmosis (ICEO) fluxes [46].

On the other hand, the good agreement between the high frequency plateaus of the birefringence of Agnws at the two concentrations confirms that particle-particle interactions can be ruled out. The same occurs in the case of confined Agnws/HFE. We also observe that the spectra in the case of confined particles reach smaller values of the Kerr constant, as it was expected in view of Fig. 5a, and it is a consequence of the difference between the electric birefringence saturation values.

The Kerr constant can be used to calculate the electric polarizability anisotropy $\Delta\alpha^e$. First, the orientational order parameter S can be calculated from the data in Table 1 and Eq. (2). From S, $\Delta\alpha^e$ can be readily obtained with the aid of Eq. (15). The results are shown in Fig. 8b. We observe similar spectra to those already reported [39]. For slender metallic particles of length L and diameter D it has been shown that there is a frequency dispersion of $\Delta\alpha^e$ [38,39,44]:

$$\mathrm{Re}\left(\frac{\Delta\alpha^e}{V_p\epsilon_0\epsilon_m}\right) = \frac{2\rho^2}{3\ln\rho}\frac{\omega^2/\omega^2_{EDL}}{1+\omega^2/\omega^2_{EDL}} \tag{16}$$

being $\rho = L/D$ the aspect ratio, $\omega = 2\pi\nu$, $\omega_{EDL} = \frac{2K_W}{DC_{EDL}\ln\frac{L}{D}}$, $\epsilon_0\epsilon_m$ is the electrical permittivity of the solution, $C_{EDL} = \epsilon_0\epsilon_m\kappa$ the capacitance of the electric double layer (EDL), and κ the inverse of the Debye length (or EDL thickness).

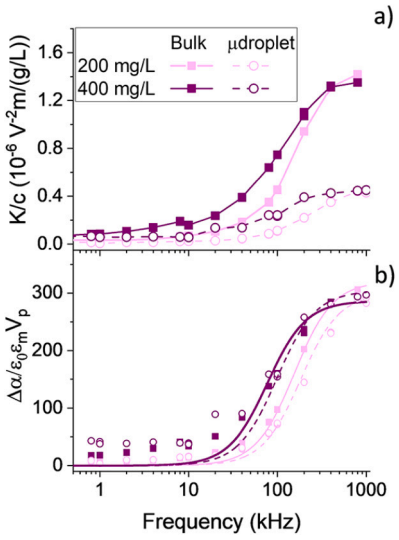

Fig. 8. a) Kerr constant of Agnws and Agnws/HFE normalized by the particle concentration c as a function of the frequency of the applied field. Lines are guides for the eye. b) Same as a) but for the electric polarizability anisotropy normalized by the permittivity of the medium and the particle volume. Lines are the best fit of Eq. (16) to the experimental data. The concentrations are Agnws 200 mg/L (NaCl 0.3 mM, pink symbols) and Agnws 400 mg/L (NaCl 0.1 mM, purple symbols). The amplitude of the applied fields were 8 V/mm (bulk samples) and between 15 and 20 V/mm (emulsions). The experimental errors are below 5% in all cases.

Table 2
Capacitance of the EDL of Agnws obtained from the experimental spectra of the Kerr constant in Fig. 8b and Eq. (16).

System	C_{EDL} (F/m^2)	λ'
Agnws 200 mg/L	0.047 ± 0.002	1.15 ± 0.05
Agnws 400 mg/L	0.031 ± 0.003	1.31 ± 0.11
Agnws/HFE 200 mg/L	0.037 ± 0.002	0.90 ± 0.05
Agnws/HFE 400 mg/L	0.030 ± 0.004	1.21 ± 0.15

In Fig. 8b we also show the theoretical expectations by fitting with Eq. (16). We observe a good agreement except for Agnws/HFE with particle concentration 400 mg/L, where the viscous torque, not included in this model, has an important effect at low frequency.

The relaxation frequency can be used to calculate the capacitance of the electric double layer C_{EDL} (see Table 2). We can use a factor λ' to quantify the deviations of the double layer capacitance from the linear relation $C_{theor,EDL} = \varepsilon_0 \varepsilon_m \kappa = C_{exp,EDL}/\lambda'$. The results are also detailed in Table 2. We observe only small deviations, and they have been previously justified by the nonlinear character of the differential capacitance [59–61]. Note also that no effect of the confinement is observed, a reasonable result since the particle polarization occurs in the electric double layer, with a size of about 20-30 nm.

3.6. Electric birefringence spectra of NaMt

In Fig. 9a we show the Kerr constant spectra of NaMt and NaMt/HFE56. It can be observed that the response of the particles inside the microdroplets is weaker, as it was already discussed in a previous section, due to the decrease in the number of particles that can be effectively oriented. Note that the maximum birefringence is obtained at high frequency and that the frequency dispersion is similar in both cases, and to that found in [38]. There, it was discussed that the particle electro-orientation is due to both an electric and a viscous torque. The first one is due to the electric polarizability anisotropy of the particles. When non-conducting particles are charged, the electric polarizability does not vanish at low frequency because it has an added contribution:

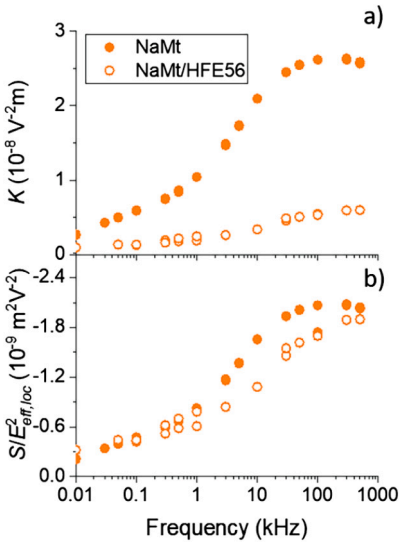

Fig. 9. a) Kerr constant of NaMt and NaMt/HFE56 as a function of the frequency of the applied field. b) Same as a) but for the orientational order parameter S normalized to the square of the applied field. Particle and NaCl concentrations are 1 g/L and 0.3 mM, respectively. The amplitude of the applied fields were 8 V/mm (bulk samples) and between 20 and 25 V/mm (emulsions). The experimental errors are below 5% in all cases.

the polarization of the EDL. Two contributions are expected: below the MHz range, ions in the EDL redistribute around the particle, this producing the so-called Maxwell-Wagner-O'Konski (MWO hereafter) relaxation. By decreasing the frequency to the kHz range a second contribution appears: a neutral electrolyte concentration gradient beyond the EDL is formed, this deforming the double layer and reducing the polarizability, in the so-called α-relaxation. This relaxation occurs at a characteristic frequency $\omega_\alpha \approx R^2/D_{dif}$ (D_{dif} is the diffusion coefficient of ions in the EDL), roughly in the kHz range. Finally, in the kHz to Hz frequency range an uneven accumulation of NaMt particles around the bigger ones takes place, and this produces a non-centrosymmetric viscous drag on the particles [33,38]. All these phenomena obey the Kerr law for weak external fields, and hence, $S \propto E^2_{eff,loc}$ throughout the whole spectra. Further details can be found in [31,34,38,41,62].

In order to study further consequences of confinement, beyond its effect on the particle concentration and electric field reduction, we can analyze $S/E^2_{eff,loc}$, which does not depend on any of these quantities. $S/E^2_{eff,loc}$ is represented in Fig. 9b as a function of the frequency of the latter. Note that in this case, since particles are oblate, the symmetry axis is the shortest one, which tends to be perpendicular to the external field. This means that S is negative. In the Kerr regime, S is proportional to the square of the electric field intensity, so the data in Fig. 9b are independent of its value. We can observe that there is not a significant influence of the confinement on the orientational order parameter of the particles, and hence it can be concluded that not only the polarizability of the particles but also the hydrodynamic flows around them must be short range effects.

4. Conclusions

In this work we have shown that the behaviour of non-spherical nanoparticles immersed in microdroplets can be measured through electric birefringence techniques, capable of determining the rotational diffusion dynamics of the confined particles and their response to an oscillating electric field, while being insensitive to the presence of the emulsion itself. Compared to other studies in literature (Ref. [16]), the present method has the advantage that it is capable of providing an in-situ analysis of nanoparticles, not visible with the microscope. Also, we have demonstrated that particles inside the droplets are effectively ori-

ented by the electric field, which is only partially screened. We have also shown that with this technique the partially screened local electric field inside the droplets can be determined.

In particular, we have analyzed silver nanowires and sodium montmorillonite platelets immersed in aqueous microdroplets that have been generated via two methods: classical emulsion through vigorous homogenization and through microfluidic techniques.

In all the analyzed cases, it was observed a lower degree of orientation inside the droplets as compared to that in unbounded media, together with an increase of the randomization time that cannot be attributed to the decrease in the electric field. The confinement effects are confirmed by analyzing the emulsion produced by stirring emulsification. With this procedure, smaller droplets were obtained, and enhanced confinements effects were found, indicating that the electro-orientation process is hindered by the presence of the water/oil interface. Our results offer a new insight in such situations where a particle concentration gradient inside the microdroplets is observed (Ref. [19]) and provide new information about the dynamics of the confined particles.

In the case of silver nanowires, information about the polarizability spectrum of the individual particles could be extracted, and it was found to be very similar to that in unbounded media. The same occurs for the orientational order parameter of the clay. This can be justified by the fact that both the electric and viscous torque that act on the particles are short-range effects around the interface particle/solution, this being far smaller than the dimensions of the droplets. With our results we may open a new field in electrokinetics, offering the opportunity to analyze the electro-hydrodynamic flows inside confined systems.

The structure and behaviour of nanoparticles inside confined geometries is both a theoretical and experimental nearly unexplored field. We expect that the proposed experiments can open new applications in printing, microfabrication and many lab-on-a-chip experimental situations, in which the interaction between particles and the water/oil interface may play an important role under external field application.

CRediT authorship contribution statement

Ana Cazorla: Experiments, Methodology, Data curation, Validation, Investigation, Formal Analysis. **Sergio Martín-Martín:** Experiments. **Ángel V. Delgado:** Writing-Original draft preparation, Funding acquisition, Investigation. **María L. Jiménez:** Conceptualization, Methodology, Investigation, Writing & Editing, Funding acquisition, Supervision.

Declaration of competing interest

The authors declare that they have no known competing financial interests or personal relationships that could have appeared to influence the work reported in this paper.

Data availability

Data will be made available on request.

Acknowledgement

The authors thank Grant No. PID2021-127427NB-I00 funded by MCIN/AEI/10.13039/501100011033 and by “ERDF A way of making Europe”, Grant No. TED2021-131855B-I00 funded by MCIN/AEI/10.13039/501100011033 and European Union Next Generation EU/PRTR and Grant No. A-FQM-492-UGR20 funded by *Junta de Andalucía*, Spain for the financial support.

Appendix A. Supplementary material

Supplementary material related to this article can be found online at https://doi.org/10.1016/j.jcis.2023.11.180.

References

[1] G. Davies, J. Stokes, Thin film and high shear rheology of multiphase complex fluids, J. Non-Newton. Fluid Mech. 148 (1–3) (2008) 73–87.
[2] G. Vleminckx, C. Clasen, The dark side of microrheology: non-optical techniques, Curr. Opin. Colloid Interface Sci. 19 (6) (2014) 503–513.
[3] J. Rubi, D. Reguera, Thermodynamics and stochastic dynamics of transport in confined media, Chem. Phys. 375 (2–3) (2010) 518–522.
[4] G. Schatz, B. Dobberstein, Common principles of protein translocation across membranes, Science 271 (5255) (1996) 1519–1526.
[5] G. Rivas, F. Ferrone, J. Herzfeld, Life in a crowded world: workshop on the biological implications of macromolecular crowding, 2004.
[6] S.-Y. Teh, R. Lin, L.-H. Hung, A.P. Lee, Droplet microfluidics, Lab Chip 8 (2008) 198–220.
[7] P. Basuri, L.E. Gonzalez, N.M. Morato, T. Pradeep, R.G. Cooks, Accelerated microdroplet synthesis of benzimidazoles by nucleophilic addition to protonated carboxylic acids, Chem. Sci. 11 (47) (2020) 12686–12694.
[8] J.K. Lee, D. Samanta, H.G. Nam, R.N. Zare, Micrometer-sized water droplets induce spontaneous reduction, J. Am. Chem. Soc. 141 (27) (2019) 10585–10589.
[9] C.K. Terry Weatherly, M.W. Glasscott, J.E. Dick, Voltammetric analysis of redox reactions and ion transfer in water microdroplets, Langmuir 36 (28) (2020) 8231–8239.
[10] C.F. Chamberlayne, R.N. Zare, Simple model for the electric field and spatial distribution of ions in a microdroplet, J. Chem. Phys. 152 (18) (2020) 184702.
[11] X. Mao, M. Wang, S. Jin, J. Rao, R. Deng, J. Zhu, Monodispersed polymer particles with tunable surface structures: droplet microfluidic-assisted fabrication and biomedical applications, J. Polym. Sci. 60 (11) (2022) 1653–1669.
[12] T. Kojima, K. Hirai, Y. Zhou, P. Weerappuli, S. Takayama, N.A. Kotov, Nanoparticle assemblies into luminescent dendrites in shrinking microdroplets, Langmuir 32 (47) (2016) 12468–12475.
[13] B. Barua, T.J. Durkin, I.M. Beeley, A. Gadh, S. Savagatrup, Multiplexed and continuous microfluidic sensors using dynamic complex droplets, Soft Matter (2023).
[14] C. Zhou, P. Zhu, Y. Tian, M. Xu, L. Wang, Engineering micromotors with droplet microfluidics, ACS Nano 13 (6) (2019) 6319–6329.
[15] S.M. Giannitelli, E. Limiti, P. Mozetic, F. Pinelli, X. Han, F. Abbruzzese, F. Basoli, D. Del Rio, S. Scialla, F. Rossi, et al., Droplet-based microfluidic synthesis of nanogels for controlled drug delivery: tailoring nanomaterial properties via pneumatically actuated flow-focusing junction, Nanoscale 14 (31) (2022) 11415–11428.
[16] M. Wozniak, G. Derkachov, K. Kolwas, J. Archer, T. Wojciechowski, D. Jakubczyk, M. Kolwas, Formation of highly ordered spherical aggregates from drying microdroplets of colloidal suspension, Langmuir 31 (28) (2015) 7860–7868.
[17] M. Bogdanova, P. Lebedev-Stepanov, Optical analysis of nanoparticle packing after drying in microdroplets, Crystallogr. Rep. 62 (2017) 966–970.
[18] P. Basuri, A. Chakraborty, T. Ahuja, B. Mondal, J.S. Kumar, T. Pradeep, Spatial reorganization of analytes in charged aqueous microdroplets, Chem. Sci. 13 (45) (2022) 13321–13329.
[19] H. Almohammadi, Y. Fu, R. Mezzenga, Evaporation-driven liquid–liquid crystalline phase separation in droplets of anisotropic colloids, ACS Nano 17 (3) (2023) 3098–3106.
[20] C. Priest, S. Herminghaus, R. Seemann, Controlled electrocoalescence in microfluidics: targeting a single lamella, Appl. Phys. Lett. 89 (13) (2006) 134101.
[21] J.-C. Baret, O.J. Miller, V. Taly, M. Ryckelynck, A. El-Harrak, L. Frenz, C. Rick, M.L. Samuels, J.B. Hutchison, J.J. Agresti, et al., Fluorescence-activated droplet sorting (fads): efficient microfluidic cell sorting based on enzymatic activity, Lab Chip 9 (13) (2009) 1850–1858.
[22] H. Zhang, A.R. Guzman, J.A. Wippold, Y. Li, J. Dai, C. Huang, A. Han, An ultra high-efficiency droplet microfluidics platform using automatically synchronized droplet pairing and merging, Lab Chip 20 (21) (2020) 3948–3959.
[23] Z. Li, B. Zhang, D. Dang, X. Yang, W. Yang, W. Liang, A review of microfluidic-based mixing methods, Sens. Actuators A, Phys. (2022) 113757.
[24] M. Chabert, K.D. Dorfman, J.-L. Viovy, Droplet fusion by alternating current (AC) field electrocoalescence in microchannels, Electrophoresis 26 (19) (2005) 3706–3715.
[25] M. Zehavi, D. Sofer, T. Miloh, O.D. Velev, G. Yossifon, Optically modulated propulsion of electric-field-powered photoconducting Janus particles, Phys. Rev. Appl. 18 (2) (2022) 024060.
[26] L.T. Yan, H.G. Schoberth, A. Böker, Large-scale oriented assembly of nanoparticles in diblock copolymer templates under electric fields, Macromol. Chem. Phys. 210 (12) (2009) 1003–1010.
[27] K.P. Loh, Q. Bao, G. Eda, M. Chhowalla, Graphene oxide as a chemically tunable platform for optical applications, Nat. Chem. 2 (12) (2010) 1015–1024.
[28] P. Arenas-Guerrero, Á.V. Delgado, S. Ahualli, M.L. Jiménez, Polymer-induced orientation of nanowires under electric fields, J. Colloid Interface Sci. 591 (2021) 58–66.
[29] M.d.M. Ramos-Tejada, J.M. Rodríguez, Á.V. Delgado, Electrorheology of clay particle suspensions. Effects of shape and surface treatment, Rheol. Acta 57 (2018) 405–413.
[30] C.T. O'Konski, Molecular Electro-Optics, Marcel Dekker, 1976.
[31] T. Bellini, F. Mantegazza, V. Degiorgio, R. Avallone, D.A. Saville, Electric polarizability of polyelectrolytes: Maxwell-Wagner and electrokinetic relaxation, Phys. Rev. Lett. 82 (1999) 5160–5163.

[32] A.M. Zhivkov, B.M. van der Zande, S.P. Stoylov, Electro-optics of metal particles: electric birefringence of gold rods, Colloids Surf. A, Physicochem. Eng. Asp. 209 (2–3) (2002) 299–303.
[33] F. Mantegazza, M. Caggioni, M.L. Jiménez, T. Bellini, Anomalous field-induced particle orientation in dilute mixtures of charged rod-like and spherical colloids, Nat. Phys. 1 (2) (2005) 103–106.
[34] M.L. Jiménez, T. Bellini, The electrokinetic behavior of charged non-spherical colloids, Curr. Opin. Colloid Interface Sci. 15 (3) (2010) 131–144.
[35] T. Robb-Smith, K. Donovan, K. Scott, M. Somerton, Induced electro-optic effects in single-walled carbon nanotubes. I. Polarizability of metallic nanotubes, Phys. Rev. B 83 (15) (2011) 155414.
[36] K. Sandhya, Influence of ZnO nanoparticles on the electric field induced birefringence of the blue phase, J. Mol. Liq. 359 (2022) 119378.
[37] H. Liang, Y. Wu, Y. Zhang, E. Chen, Y. Wei, Y. Ji, Elastomers Grow into Actuators, Advanced Materials, 2023, 2209853.
[38] P. Arenas-Guerrero, G.R. Iglesias, Á.V. Delgado, M.L. Jiménez, Electric birefringence spectroscopy of montmorillonite particles, Soft Matter 12 (22) (2019) 4923–4931.
[39] P. Arenas-Guerrero, Á.V. Delgado, A. Ramos, M.L. Jiménez, Electro-orientation of silver nanowires in alternating fields, Langmuir 35 (3) (2018) 687–694.
[40] E. Fredericq, C. Houssier, Electric Dichroism and Electric Birefringence, Clarendon, Oxford, 1973.
[41] V. Shilov, T. Simonova, Polarization of electric double-layer of disperse particles and dipolophoresis in a steady (DC) field, Colloid J. USSR 43 (1) (1981) 90–96.
[42] M.Z. Bazant, T.M. Squires, Induced-charge electrokinetic phenomena: theory and microfluidic applications, Phys. Rev. Lett. 92 (6) (2004) 066101.
[43] T.M. Squires, M.Z. Bazant, Breaking symmetries in induced-charge electro-osmosis and electrophoresis, J. Fluid Mech. 560 (2006) 65–101.
[44] J.J. Arcenegui, P. García-Sánchez, H. Morgan, A. Ramos, Electro-orientation and electrorotation of metal nanowires, Phys. Rev. E 88 (6) (2013) 063018.
[45] J.J. Arcenegui, P. García-Sánchez, H. Morgan, A. Ramos, Electro-orientation of a metal nanowire counterbalanced by thermal torques, Phys. Rev. E 89 (6) (2014) 062306.
[46] A. Ramos, P. García-Sánchez, H. Morgan, Ac electrokinetics of conducting microparticles: a review, Curr. Opin. Colloid Interface Sci. 24 (2016) 79–90.
[47] I. Dozov, C. Goldmann, P. Davidson, B. Abécassis, Probing permanent dipoles in CdSe nanoplatelets with transient electric birefringence, Nanoscale 12 (20) (2020) 11040–11054.
[48] M.M. Tirado, C.L. Martínez, J.G. de la Torre, Comparison of theories for the translational and rotational diffusion coefficients of rod-like macromolecules. Application to short DNA fragments, J. Chem. Phys. 81 (4) (1984) 2047–2052.
[49] E. Tekle, M. Ueda, Z. Schelly, Dynamics of electric field induced transient-phase separation in water-in-oil microemulsion, J. Phys. Chem. 93 (16) (1989) 5966–5969.
[50] Q. Brosseau, P.M. Vlahovska, Streaming from the equator of a drop in an external electric field, Phys. Rev. Lett. 119 (3) (2017) 034501.
[51] C.T. O'Konski, K. Yoshioka, W.H. Orttung, Electric properties of macromolecules. IV. Determination of electric and optical parameters from saturation of electric birefringence in solutions, J. Phys. Chem. 63 (10) (1959) 1558–1565.
[52] G. Schwarz, Zur theorie der leitfähigkeitsanisotropie von polyelektrolyten in lösung, J. Phys. 145 (1956) 563–584.
[53] P. Arenas-Guerrero, Á.V. Delgado, M.L. Jiménez, Analysis of the electro-optical response of graphene oxide dispersions under alternating fields, Carbon 144 (2019) 395–401.
[54] Á.V. Delgado, Interfacial Electrokinetics and Electrophoresis, vol. 106, CRC Press, 2001.
[55] J.-u. Shim, S.N. Patil, J.T. Hodgkinson, S.D. Bowden, D.R. Spring, M. Welch, W.T. Huck, F. Hollfelder, C. Abell, Controlling the contents of microdroplets by exploiting the permeability of PDMS, Lab Chip 11 (6) (2011) 1132–1137.
[56] Y. Bai, X. He, D. Liu, S.N. Patil, D. Bratton, A. Huebner, F. Hollfelder, C. Abell, W.T. Huck, A double droplet trap system for studying mass transport across a droplet-droplet interface, Lab Chip 10 (10) (2010) 1281–1285.
[57] S. Bachler, M. Ort, S.D. Krämer, P.S. Dittrich, Permeation studies across symmetric and asymmetric membranes in microdroplet arrays, Anal. Chem. 93 (12) (2021) 5137–5144.
[58] G. Etienne, A. Vian, M. Biočanin, B. Deplancke, E. Amstad, Cross-talk between emulsion drops: how are hydrophilic reagents transported across oil phases?, Lab Chip 18 (24) (2018) 3903–3912.
[59] M.Z. Bazant, M.S. Kilic, B.D. Storey, A. Ajdari, Towards an understanding of induced-charge electrokinetics at large applied voltages in concentrated solutions, Adv. Colloid Interface Sci. 152 (1–2) (2009) 48–88.
[60] M. Jiménez, S. Ahualli, P. Arenas-Guerrero, M. Fernández, G. Iglesias, A. Delgado, Multiionic effects on the capacitance of porous electrodes, Phys. Chem. Chem. Phys. 20 (7) (2018) 5012–5020.
[61] J.J. López-García, J. Horno, C. Grosse, Combined ionic size and electrode spacing effects on the differential capacitance of confined electrolytic cells, J. Phys. Chem. C 126 (21) (2022) 9154–9160.
[62] T. Bellini, F. Mantegazza, Electric birefringence spectroscopy: a new electrokinetic technique, in: A. Delgado (Ed.), Interfacial Electrokinetics and Electrophoresis, Marcel Dekker, New York, 2002, pp. 401–441.